Experimental techniques against RANS method in a fully-developed turbulent pipe flow

Historical evolution of experimental and computational techniques for the study of turbulence

Gabriela Lopez-Santana - Andrew Kennaugh - Amir Keshmiri*

Abstract Turbulence has been studied by scientists and engineers for decades as it appears in the majority of the fluids existent in nature and in engineering applications and because turbulent flow and its underlying behaviour are tremendously complex. The University of Manchester is widely viewed as the birthplace of turbulence due to the pioneering work of one of its prominent academics, Professor Osborne Reynolds (1842-1912). Building on this legacy, a classical experimental apparatus has been used in this paper to study a turbulent pipe flow with the aim of measuring the mean velocity field and wall shear stress using four experimental techniques, all developed in the 20th century, namely static pressure drop; mean square signals measured from a hot-wire; Preston tube; and the 'Clauser Plot'. The experimental results have then been compared against those obtained using Computational Fluid Dynamics (CFD), utilising different two-equation turbulence models. The present work highlights the discrepancies evident in obtaining the value of the wall shear stress in each method. In addition, the scopes and limitations of each technique are discussed in detail, highlighting the clear evolution of turbulence study tools over the last 100 years.

Keywords: CFD - experimental fluid mechanics - fully-developed pipe flow - turbulence - Preston tube - Clauser plot

Nomenclature

$\overline{E_{ac}}$	mean voltage alternating current	[V]
$\bar{E}$	mean voltage across the hot-wire	[V]
$\overline{u'}$	mean velocity fluctuation	[m/s]
$\bar{U}$	mean velocity	[m/s]
$\mathrm{A_c}$	cross sectional area of the pipe	[m^2]
$\mathrm{C_f}$	wall skin friction coefficient	
D	outer diameter of Preston tube	[m]
d	inner diameter of Preston tube	[m]
E	voltage across the hot-wire	[V]
E_1	output voltage of the 45º hot-wire anemometry in positive traverse	[V]
E_2	output voltage of the 45º hot-wire anemometry in negative traverse	[V]
E_{rms}	root mean square voltage	[V]
k	turbulent kinetic energy	[m^2/s^2]
L	distance between static tapping points	[m]
l	characteristic length	[m]
l_m	mixing length	[m]
n	power-law exponent	
R	pipe radius	[m]
r	distance from the centre	[m]
Re	Reynolds number	
Re_c	critical Reynolds number	
U	total velocity	[m/s]
U^+	dimensionless velocity	
U_τ	shear velocity	[m/s]
U_m	maximum velocity at the centre line	[m/s]
U_{rms}	root mean square velocity	[m/s]

* Gabriela Lopez-Santana - Andrew Kennaugh - Amir Keshmiri (✉)
Department of Mechanical, Aerospace and Civil Engineering (MACE), The University of Manchester
Manchester, M13 9PL, United Kingdom
Tel.: +44(0)161 306 5752
email: a.keshmiri@manchester.ac.uk

Y^+	dimensionless near wall distance	
ΔP	pressure differences	[Pa]
μ	coefficient of dynamic viscosity	[Ns/m^2]
ν	coefficient of kinematic viscosity	[m^2/s]
ω	specific rate of dissipation	[l/s]
ρ	density	[kg/m^3]
τ	total shear stress	[Pa]
τ'_{xy}	Reynold shear stress measured by a hot-wire method	[Pa]
$\tau_{w_{PD}}$	wall shear stress measured by the static pressure drop method	[Pa]
τ_w	wall shear stress	[Pa]
ε	turbulence dissipation rate	[m^2/ s^3]
k_{hw}	hot-wire calibration coefficient	[V/m/s]

1 Introduction

1.1 Background

Turbulent flow is amongst the most studied subjects in fluid dynamics, largely due to its presence across a wide variety of applications. A flow is characterised as turbulent when the Reynolds number exceeds a critical value. The critical Reynolds number, as well as the characteristic length, are case-specific parameters. Common environmental and industrial applications are associated with augmented Reynolds numbers which characterise the flow regime as turbulent [1]. The present investigation aims to study the behaviour of the fluid inside a pipe: air was forced to flow inside by the action of an upstream fan for the quantification of the mean velocity field and the estimation of shear stresses of fully-developed turbulent flow. An additional purpose of this work is to highlight the evolution of turbulent flow analysis tools by applying common experimental and computational techniques.

Specifically, hot-wire anemometry [2] was used to measure the mean and fluctuating properties of a turbulent flow, while the wall shear stress was measured using four different methods: a) Static pressure drop over a known length of pipe [3]; b) Mean square signals from a hot-wire [4]; c) Preston Tube [5,6]; and, d) The law of the wall (Clauser Plot) [7,8]. The velocity and viscosity measurements were further analysed with attention given to the distribution across the pipe. The commercial CFD software, ANSYS Fluent[9], was used to numerically simulate the turbulent fluid flow in the pipe. The results of all the methods used here are discussed in detail, outlining from historical and practical perspectives the evolution of techniques available for a fluid dynamicist studying the complex phenomena involved in turbulent flows.

1.2 Historical Evolution of the Experimental and Computational Techniques

Experimental techniques have been used to study turbulent flows for many decades. The experimental work of Professor Reynolds [10] in the late 19th century at the University of Manchester contextualised the parameters associated with turbulent flows. A substantial number of studies have specifically examined turbulent pipe flows and it is of particular interest to note the evolution of these methods over time. The static pressure drop method, based on the fundamental theory of fluid mechanics, has been applied for the wall shear stress calculation since the introduction of pressure tapping techniques in 1888 [17]. Hot-wire anemometry was introduced at the beginning of the 20th century based on the theoretical work of Boussinesq in 1905 [18] and Russel in 1911 [19], although the first actual experiments were not conducted until the 1910s, most notably in the significant work of King in 1914 [20]. Subsequently, research on the measurement of fluctuating turbulent velocity with hot-wires in 1929 [21] enabled the application of hot-wire anemometry for the calculation of the wall shear stresses. In 1954, Preston [6] developed a new approach on the principle that the surface shear stress can be accurately predicted by modified Pitot tubes of different sizes. Finally, the law of the wall, also known as the Clauser Plot, was introduced in 1956 [7] offering a graphic approach for approximating the wall shear stress.

Since 1969, computational techniques have discretised the Navier-Stokes equations in space and time in order to investigate turbulent effects [11]. However, due to the very fine structures associated with turbulent flows, the analytical solution offered by the Navier-Stokes equations is hardly feasible [12]; nevertheless, in many cases, the fine turbulent structures may be of low interest. As such, approximation models have been developed for the estimation of turbulent flow fields [13–16]. The first computational technique examining turbulence was the Large Eddy Simulation (LES), introduced in 1970 by Deardorff [16]. In 1972, Orszag and Patterson developed the first Direct Numerical Simulation (DNS) for low Reynolds number [22]. Despite their high level of detail, they are limited by their requirements of supercomputers and by their computational times, which are excessively long for everyday applications [23]. Launder and Spalding presented the Reynolds-averaged Navier-Stokes (RANS) in 1972, which went on to become the most common technique to model turbulence, even until today. Its improved efficiency has made the RANS method the standard tool for turbulence modelling for most engineering applications [24–30].

1.3 Aims and Objectives

The main aim of the present work is to assess the accuracy of four classical experimental techniques, all developed in the 20th century for measuring the mean velocity field and wall shear stress for a fully-developed pipe flow. The experimental data are then compared against the CFD results utilising a two-equation eddy-viscosity turbulence model to provide an assessment on the performance of historic experimental techniques with one of the latest computational simulations.

2 Methods

2.1 Test Rig and Instrumentation

The experimental set-up used in the present study is located in the premises of The University of Manchester, shown in Fig. 1. It consists of:

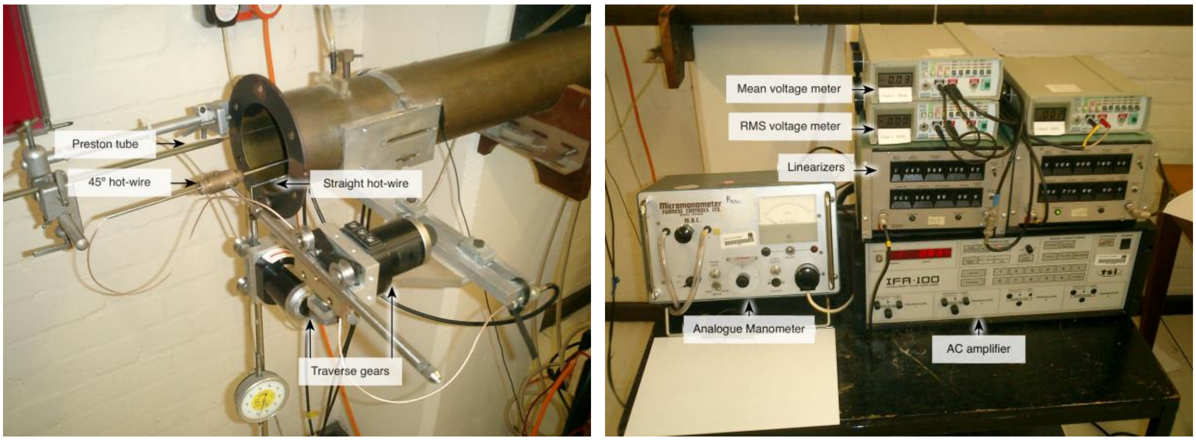

(a) Equipment at the pipe exit. (b) Digital devices used in this experiment.

Fig. 1: Test rig for the study of fully-developed turbulent flow in a pipe.

- A brass pipe with length to diameter ratio of 125:1. This length to diameter ratio is considered adequate for a high Reynolds number.
- A variable speed centrifugal fan that is used at the inlet and forces air at ambient conditions to flow along the pipe.
- An analogue manometer which is connected via a pressure switch to static pressure tapings in the wall of the pipe and also to a Preston tube placed at the pipe exit.
- A Preston tube that is used at the outlet of the brass pipe in order to measure the dynamic pressure.
- Static pressure tappings that are used at two points on the wall of the pipe to calculate the pressure drop along the pipe over a fixed distance.
- A set of two pressure switches that are used to interconnect a digital manometer apparatus with the Preston tube.
- A hot-wire anemometer.

2.2 Instrumentation and Measurements

2.2.1 Anemometry measuring system

- Two single hot-wire probes (one straight and one 45^0 hot-wire).
- A set of traverse gears are implemented to move the hot-wire to the required position in the pipe.
- Two Constant Temperature Anemometer (CTA) bridges.

- A linearizer is used to enhance the non-linear behaviour of the amplifier and to filter down a portion of the noise interfering with the output data from hot-wire anemometry which is mainly caused by the fluctuation of the probe in the pipe.
- The mean and the Root Mean Square (RMS) velocities are measured by two separate voltage meters.
- Two digital voltmeters.
- AC amplifier for increasing the signal of the time-varying voltage.

2.2.2 Hot-Wire Anemometer

Hot-wire anemometers have been widely used to measure velocities, especially those with high frequency velocity fluctuations, i.e. turbulence [31]. A hot-wire anemometer consists of a sensor used to measure the change of velocities rapidly with good spatial and time resolution and comprises a metallic (usually tungsten) filament of a micron in diameter [32] that has a known and constant variation of resistance with temperature. This filament is welded to metallic prongs of much larger diameter and the filament length is typically of the order of 2 - 3mm long depending on the probe design. When used, the hot-wire probe is placed in air streams and is heated by passing a small electric current through it and some of the heat generated by Joule effect in the filament is absorbed by the air flow via convection [33]. This cooling effect changes the resistance of the wire and thus provides a means of measuring the flow since the change of resistance reflects the flow velocity. There are two main types of hot-wire anemometer, namely the constant current (CCA) and constant temperature (CTA); the latter is more common. In operation, the CCA is continuously cooled by the flow and this ultimately leads to the sensitivity decreasing as the wire temperature approaches ambient at high velocities. With the CTA, there is a servo electrical system consisting of a Wheatstone bridge that responds to the change of resistance of the hot-wire by either increasing or decreasing the power to it according to whether it is too cold (high velocity) or too hot (low velocity) [34]. This change of power is measured as a change of voltage that can be directly related to the flow velocity by suitable calibration [33]. It is essential that the hot-wire does not make contact with the pipe wall, as this renders it ineffectual; it was observed that the hot-wire measurements near to the wall increase the zero volts and any subsequent measurement produces an error [35] and also that the hot-wire is shorted out if both prongs touch the wall. The hot-wire probes here were used with an Analogue to Digital Converter (ADC) and a computer control, which allowed fluctuations in time to be recorded from the sensor.

2.3 Experimental Procedure

2.3.1 Measurement of the Velocity Field

The hot-wire was positioned so that measurements of the mean and RMS velocities could be appropriately acquired from a distance as close to the wall as possible using the digital voltmeters. The only way to ensure positional accuracy is to connect a voltmeter to measure the resistance between the hot-wire and the brass tube. The contact between them means that it is at the wall (i.e. 0mm). Preliminary measurements were taken from an initial distance of 0.1mm from the wall and, subsequently, several measurements were taken along the radius of the tube up to the centre-line, enabling the average Reynolds number, which determines the regime of the flow in the pipe, to be calculated. Usually, without using the linearizer, the calibration follows King's law [36].

$$E^2 = A + Bu^n \tag{1}$$

Where E is the voltage along the hot-wire, u is the velocity of the normal flow of the wire and A, B and n are constants.

In this experiment, the straight hot-wire was pre-calibrated with a linear calibration coefficient k_{hw} equal to 0.5 V/ms^{-1} applied to the hot-wire output. The calibration coefficient is non-linear, however here a linear slope is assumed, meaning that, to calculate the velocity components, the readings from the voltmeter need to be multiplied by a factor of two. The required velocities were obtained as follows:

$$\overline{U} = \overline{E_{ac}}\frac{1}{k_{hw}} \tag{2}$$

$$U_{rms} = E_{rms}\frac{1}{k_{hw}} \tag{3}$$

$$U = \overline{U} + U_{rms} \tag{4}$$

Equation (4) adopts the Reynolds decomposition, which represents the instantaneous velocity as a summation of the mean (time-averaged) velocity and the fluctuating velocity. The convention of associating the x-axis with the mean velocity and y-axis with the direction traverse to the supports is used to represent the velocity. It is worth noting that the methods introduced above are only valid when the flow in the pipe is fully-developed and turbulent. Thus, to verify this condition, it is necessary to initially calculate the Reynolds number using the non-dimensional Reynolds equation:

$$Re = \frac{\rho U D_{pipe}}{\mu} \tag{5}$$

The distribution of the velocity profile gives a reliable illustration of the main features of the turbulent flow and can be compared with the data collected in experiments utilising dimensionless analysis. Dimensionless velocities indicate that there is a general solution of the velocity profile applicable for all fluid and is calculated as follows:

$$U^{+} = \frac{U}{U_{\tau}} \tag{6}$$

where the shear velocity, U_{τ}, is defined as:

$$U_{\tau} = \sqrt{\frac{\tau_w}{\rho}} \tag{7}$$

where τ_w is the wall shear stress and ρ is the density. The dimensionless near wall distance, Y^{+}, is defined as:

$$Y^{+} = \frac{yU_{\tau}}{\nu} \tag{8}$$

where y is the distance to the nearest wall and ν is the kinematic viscosity.

2.3.2 Power-law velocity profile

The power-law velocity profile is used to represent turbulent flow in a pipe. The empirical relation is obtained as:

$$\frac{\overline{U}}{U_m} = \left(1 - \frac{\mathrm{r}}{\mathrm{R}}\right)^{\frac{1}{\mathrm{n}}} \tag{9}$$

where $\overline{U}$ is the mean velocity, U_m is the maximum velocity at the centre line, r is the distance from the pipe centre, R is the total radius of the pipe in this case $R = 51mm$ and n is a constant exponent that depends on the Reynolds number. The empirical one-seventh power-law declares that the value of $n = 7$ approximates most of the flows [37].

Method 1: Static Pressure Drop

The static pressure drop method, available for fully developed internal flows and axisymmetric conditions, enables the measurement of the average wall shear stress from the axial pressure gradient. The pressure drop is measured with the use of two static pressure tapings along the pipe. The shear stress $\tau_{w_{PD}}$ for a fully developed circular pipe acting over a surface area A is related with the pressure drop ΔP over a length L of a constant cross-sectional area A_c by:

$$\int_A \tau_{w_{PD}}\, dA = \Delta P A_c \tag{10}$$

$$\tau_{w_{PD}} = \frac{\Delta P \pi R^2}{2\pi R L} = \frac{\Delta P}{2L} R \tag{11}$$

Harotinidis [38] suggested that this method is perhaps the most reliable for flows satisfying the conditions listed above. In fact, only flows in a circular pipe would meet the above conditions; and, even for a fully developed pipe flow, this method affects the accuracy of the measurement, due to the size of the pressure tap and the quality of the tap hole [39].

Method 2: Mean Square Signal (45° Hot-wire)

The slanted hot-wire is sensitive to the components of the velocity fluctuation of turbulent and/or unsteady flow. The wire orientation with respect to the mean flow vector and wire cooling laws vary the sensitivity coefficients, *A*. The equation that describes the heat transfer of the hot-wire can be linearized to establish a relation between the anemometer voltage fluctuation, *E*, and the velocity fluctuations, u', v', w', if these fluctuations are minor [39].

$$E = A_u u' + A_v v' + A_w w' \tag{12}$$

After squaring and averaging the equation, the mean value of the anemometer fluctuations can be found:

$$\overline{E^2} = {A_u}^2\overline{u'^2} + {A_v}^2\overline{v'^2} + {A_w}^2\overline{w'^2} + 2A_uA_v\overline{u'v'} + 2A_uA_w\overline{u'w'} + 2A_vA_w\overline{v'w'} \tag{13}$$

Deriving the sensitive coefficients of a slanted hot-wire and assuming steady flow and simple cooling laws, the heat transfer of a hot-wire by an effective velocity can be described by King's law, where the slope represents the sensitivity [36].

In this method, the wall shear stress was estimated using a single 45^0 hot-wire in reversed horizontal attitudes, positioned half a diameter upstream of the pipe exit. The initial probe position was set to $10mm$ from the wall and then traversed the diameter of the pipe towards the centre line, using pre-defined increments. A second set of measurements was taken at the same positions with the probe rotated 180^0. On this occasion, the probe traversed the diameter of the pipe from the centreline towards the wall until it reached the distance of $10mm$ from the wall. The RMS voltages were measured with the 45^0 hot-wire, which translate the RMS velocities. The two traverses in the horizontal plane, E_1 and E_2, correspond to the instantaneous voltage applied across the hot-wire [34].

$$\overline{u'v'} = \frac{E_2^2 - E_1^2}{2k_{hw}^2} \tag{14}$$

Where $\overline{u'v'}$ represents the time average of the product of the fluctuating velocity components u' and v' and has the dimension of velocity squared; k_{hw} is the calibration coefficient mentioned earlier.

Due to the eddy motion of the particles of the fluid, the Reynolds shear stress can be interpreted as the shear force per unit area and, to calculate the wall shear stress, the following equation can be used:

$$\tau'_{xy} = \rho\ \overline{u'v'} \tag{15}$$

the boundary conditions applied at the wall are: $(\overline{u'v'})_{wall} = 0$ and $k_{wall} = 0$.

Based on McDonough's work [41] demonstrating that the shear stress is a linear function of the variable radius *r* and the wall shear stress, the value of the shear stress can also be obtained through:

$$\tau = \tau_w \frac{r}{R} \tag{16}$$

Method 3: Preston Tube

The wall shear stress was also measured with the use of a Preston tube, positioned so that its outer surface was tangential to the pipe inner wall while facing upstream. With appropriate configuration of the analogue manometer, the dynamic pressure can be taken. Theoretically, with the Preston tube, the wall shear stress is related to the dynamic pressure as:

$$\left[\frac{\rho\tau_w d^2}{\mu^2}\right] = f\left[\frac{\rho\Delta P d^2}{\mu^2}, \frac{d}{D}\right] \tag{17}$$

where d and D are the internal and external diameters of the Preston tube respectively. As the Preston tube is a thick-walled tube, it tends to give the most reproducible behaviour because it matches the skin friction with the data of the stagnation pressure from the tube placed at the wall.

Historical tests have established relationships between the wall shear stress τ_w and the dynamic pressure ΔP, defined as the mean difference between the pressure sensed by the Preston tube and the static pressure obtained from a nearby wall tap [39].

In this case, where $\frac{d}{D} = 0.6$, the following widely accepted analytical relationships were obtained [42]:

$$\begin{gathered} 0 < X^* < 2.9 \\ Y^* = X^* + 0.037 \end{gathered} \tag{18}$$

$$\begin{gathered} 2.9 < X^* < 5.6 \\ Y^* = 0.827 - 0.1381X^* + 0.1437X^{*^2} - 0.006\, X^{*^3} \end{gathered} \tag{149}$$

$$\begin{gathered} 5.6 < X^* < 7.6 \\ Y^* = 2\ \ log_{10}(1.95X^* + 4.10) + X^* \end{gathered} \tag{20}$$

where

$$X^* = log_{10}\left[\frac{\rho\Delta P d^2}{4\mu^2}\right] \tag{151}$$

Having prescribed X^* and determined Y^+, the wall shear stress can then be defined as:

$$\tau_w = \frac{4\ (10^{Y^*})\mu^2}{\rho d^2} \tag{162}$$

Method 4: Clauser Plot

In turbulent flows over smooth surfaces, there is always a sub-layer next to the wall in which the flow is laminar, since a solid surface tends to damp out the turbulent fluctuations. Nevertheless, within the viscous sub-layer and the inner region (which is a fully turbulent flow region), the turbulent stress is zero. In the log-law region at the inner region, the dimensionless velocity is represented in the logarithmic form (see Fig.2b) as:

$$U^+ = \frac{1}{\kappa}\ln Y^+ + B \tag{17}$$

where κ is the Von-Karman constant and is assumed $\kappa = 0.41$, and $B = 5.3$ [7,8]. This form of velocity distribution is widely used in turbulent pipe flow and is known as the "Universal Law of the Wall" [41].

The Clauser plot is a graphical method used to estimate the turbulent wall shear stress from its correlation with the law of the wall. Equation (23) can be rearranged and presented in a normalised form to obtain the wall shear stress, using the properties of the velocity profile in the logarithmic part of the boundary layer [43]:

$$\frac{U(r)}{U_\tau} = \frac{1}{\kappa}\ln\left(\frac{yU_\tau}{\nu}\right) + B \tag{184}$$

Multiplying both sides by $\frac{U_\tau}{U_m}$ gives:

$$\frac{U(r)}{U_m} = \left[\frac{1}{\kappa}\frac{U_\tau}{U_m}\right]\ \ln\left(\frac{yU_m}{\nu}\right) + \left[\frac{1}{\kappa}\frac{U_\tau}{U_m}\ln\left(\frac{U_\tau}{U_m}\right) + B\,\frac{U_\tau}{U_m}\right] \tag{195}$$

where, as indicated previously, the friction velocity is equal to: $U_\tau = \sqrt{\frac{\tau_w}{\rho}}$ and noting that the friction coefficient is given by:

$$C_f = 2\left(\frac{U_\tau}{U_m}\right)^2 \tag{26}$$

The Clauser plot equation can be rewritten as follows:

$$\frac{U(r)}{U_m} = \left[\frac{1}{\kappa}\sqrt{\frac{C_f}{2}}\right] \ln\left(\frac{yU_m}{\nu}\right) + \left[\frac{1}{\kappa}\sqrt{\frac{C_f}{2}} \ln\left(\sqrt{\frac{C_f}{2}}\right) + B\sqrt{\frac{C_f}{2}}\right] \tag{27}$$

κ and B are constants and the velocity terms can be obtained from the experiment, leaving only the friction coefficient as an unknown.

The value of the friction coefficient C_f is estimated graphically when different values are superposed in the semi-logarithmic plot of $\frac{U}{U_m}$ vs $\frac{U_m y}{\nu}$ [44] and will be further discussed in Section 3.1.2. Therefore, the wall shear stress can be obtained by rearranging equation (26) and replacing the friction velocity from equation (7):

$$\tau_w = \frac{\rho U_m^2 C_f}{2} \tag{208}$$

2.4 Computational Method

In the present work, the fully-developed turbulent pipe flow was simulated computationally using the most popular commercial CFD package, ANSYS Fluent. The length of the pipe in the experiment was required to be as long as $L = 125D$ to ensure a fully-developed turbulent flow. The present computational domain consists of a cylindrical segment of length $4mm$ and diameter $102mm$, simulated using a periodic boundary condition. This significantly reduces the computational time, and also takes advantage of the axisymmetric pipe. At the entrance of the pipe, an estimated mass flow rate of $\dot{m} = 7.5x10^{-2}kg/s$ is translated into a velocity of $7.5m/s$, which is equally distributed along and normal to the inlet surface.

In this experiment the Reynolds number was notably high $Re = 57469$, so the assumption of a turbulent regime is valid. A turbulence intensity of 10% is assumed at the inlet. No slip-boundary conditions were applied on the pipe wall. A static pressure boundary condition of zero pascals was set at the outlet.

2.4.1 Grid Generation

A multi-block grid was generated from the 3D circular pipe computational domain and was divided in two sub-regions: a central square region and an exterior circular region. Accurate representation of the viscous sublayer is required for a satisfactory prediction of wall-bounded turbulent fluids. The first cell height was calculated using equation (8). The mesh must be finest around the wall and become progressively coarser towards the central square region, with an aspect ratio of 1.2. The stream-wise direction does not require an excessive number of cells. In order to analyse grid independency, four different grid resolutions were compared as shown in Table 1.

Table 1: Comparative table of 3D Multiblock/Hexahedral grid method.

Coarse mesh	Medium mesh	Fine mesh	Very fine mesh
3060 cells	9520 cells	30240 cells	90045 cells
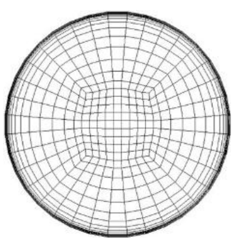	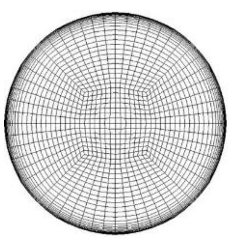	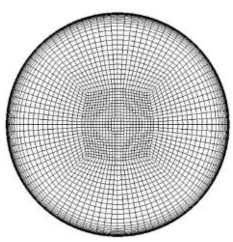	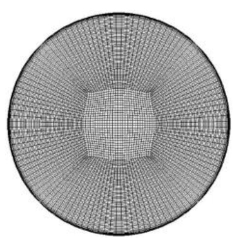

2.4.2 Turbulence Modelling

Turbulence modelling is a crucial methodological aspect of any CFD simulation and it significantly affects the final results. In theory, the Navier-Stokes equations are adequate for simulating a turbulent flow, but, due to the small size and fine detail of the turbulent structures and the consequent demand for a very fine domain discretization, the Direct Numerical Simulation (DNS) is deemed computationally unaffordable. To overcome these profound limitations, turbulence models have been developed in which the eddies are approximated either by an averaged flow field (RANS approach) or by limiting the size of the eddies which are modelled (Large Eddy Simulation (LES)). The turbulence model to approximate the eddies by an averaged flow field used in this work is the RANS approach, since it is the most computationally inexpensive and offers a good representation of the flow field [24].

Several RANS models have been introduced in the last decades and applied in demanding CFD applications (e.g. [46–50]). In this study, the $\kappa - \omega - SST$ (Shear Stress Transport) turbulence model is used, which is a combination of the $\kappa - \omega$ and the $\kappa - \varepsilon$ turbulence models as proposed by Menter [51]. In this model, the $\kappa - \omega$ formulation is implemented in the inner region of the boundary layer and it is substituted by $\kappa - \varepsilon$ model for the free shear region of the flow.

In the $\kappa - \omega - SST$ model, the turbulent kinetic energy κ and the specific rate of dissipation ω are expressed through the following differential equations:

$$\frac{\partial k}{\partial t} + U_j \frac{\partial k}{\partial x_j} = P_k - \beta^* k\omega + \frac{\partial}{\partial x_j}\left[(\nu + \sigma_k \nu_T)\frac{\partial k}{\partial x_j}\right] \tag{29}$$

$$\frac{\partial \omega}{\partial t} + U_j \frac{\partial \omega}{\partial x_j} = \alpha S^2 - \beta\omega^2 + \frac{\partial}{\partial x_j}\left[(\nu + \sigma_\omega \nu_T)\frac{\partial \omega}{\partial x_j}\right] + 2(1 - F_1)\sigma_{\omega_2}\frac{1}{\omega}\frac{\partial k}{\partial x_i}\frac{\partial \omega}{\partial x_i}$$

where the eddy viscosity, ν_T is expressed as:

$$\nu_T = \frac{a_1 k}{\max(a_1\omega, SF_2)} \tag{30}$$

while

$$F_2 = tanh\left(\left[\frac{2\sqrt{k}}{\beta^*\omega y}, \frac{500v}{y^2\omega}\right]^2\right) \tag{31}$$

$$P_k = min\left(\tau_{ij}\frac{\partial U_i}{\partial x_j}, 10\beta^* k\omega\right) \tag{32}$$

$$F_1 = \tanh\left(\left[min\left(max\left[\frac{\sqrt{k}}{\beta^*\omega y^2}, \frac{500\,v}{y^2\omega}\right], \frac{4\sigma_{\omega_2}k}{CD_{k\omega}y^2}\right)\right]^4\right) \tag{33}$$

$$CD_{k\omega} = \max\left(2\rho\sigma_{\omega_2}\frac{1}{\omega}\frac{\partial k}{\partial x_i}\frac{\partial \omega}{\partial x_i}, 10^{-10}\right) \tag{34}$$

The closure constants involved in the $\kappa - \omega - SST$ model are shown in Table 2. The following boundary conditions for κ and ω are set on the wall: $k_{wall} = 0$ and $\omega_{wall} = 10\frac{6v}{\beta(\Delta d_1)^2}$

Table 2. Closure constants of the *k* – *ω* – SST model.

$\kappa - \omega$	$\kappa - \varepsilon$	SST
$\sigma_{k1} = 0.85$	$\sigma_{k2} = 1.00$	$\beta^* = 0.09$
$\sigma_{\omega 1} = 0.65$	$\sigma_{\omega 2} = 0.856$	$\alpha_1 = 0.31$
$\beta_1 = 0.075$	$\beta_2 = 0.0828$	

2.4.3 Boundary Conditions

Periodic boundary conditions are applied when the fluid across two opposite planes of the computational domain are the same [52]. For a fully-developed flow, it is not necessary to simulate the full length of the pipe so, to reduce the number of cells and the computational time, the domain simply comprised a small section of the pipe and cyclic or periodic boundary conditions were applied, meaning that the results of the outlet were the new input of the inlet. No slip-boundary conditions were applied on the pipe wall to reproduce the effects of friction with null velocity at the wall and a static pressure boundary condition of zero pascals was set at the outlet.

2.4.4 Discretization

The discretization of the partial derivative equations at the grid points use the Finite Volume Method (FVM). A second order discretization scheme for evaluating the convective and diffusive terms were selected to ensure that the solution remain bounded because it has been proven that higher order discretization schemes bring convergence problems and instability of the solution [56].

2.4.5 Pressure-Velocity Coupling Scheme

The Semi Implicit Method for Pressure Linked Equations (SIMPLE) scheme, which is broadly used in CFD simulations [53], is the one employed in the present study. There is not an equation for controlling the evolution of the pressure in the set of the Navier-Stokes equations and, for this reason, an iterative procedure is needed to relate the pressure and velocity; one disadvantage of the SIMPLE scheme is that it takes more time to converge.

2.4.6 Convergence Criteria

Due to the presence of non-linear terms (convective) in the momentum equations, convergence criteria in CFD needs to be carried out by an iterative method. A residual value was used to monitor convergence and to assess proximity to the solution. The iterations should stop when the difference between the estimated solution and the previous approximation has reached a maximum residual value [54]. The maximum residual value settled for the following simulations are 1.0 E-6.

3 Results and Discussion

The results of the experimental and computational techniques are presented and discussed in this section. First, experimental results are presented where the attention is restricted to the velocity profiles and the shear stresses distribution inside the pipe. Subsequently, the computational results are presented and compared with the experimental data.

3.1 Experimental Results

3.1.1 Velocity Profile Analysis

Fig. 2a presents the normalised velocities over the normalised distance from the wall in linear axes. In order to best illustrate the velocity distribution across the pipe, the normalised velocity $\frac{U}{U_m}$ is plotted against $1 - \frac{r}{R}$, with the maximum velocity naturally obtained at the centre line, $U_m = 8.69 m/s$. As discussed previously, in this experiment, the Reynolds number was found to be very high ($Re = 57469 \ >> \ 4000$), validating the assumption of a turbulent regime.

Fig. 2a shows the turbulent region, excluding the viscous sub-layer and its approximation by a parameter-fitted power-law curve. It illustrates that the power-law exponent n was found to be 7.48, thus deviating by approximately 7% from the one-seventh power-law rule (equation 9). It also demonstrates that the total velocity corresponds to $\approx$ 68% of the centreline velocity.

In Fig. 2b, the three characteristic regions of the turbulent boundary layer can be distinguished as viscous sub-layer, buffer layer and log-law layer, informed by a wider theoretical background on the turbulent flow field regions in the relevant literature [13,24,55]. The flow in the viscous sublayer is very close to the tube wall and it is laminar,$0 \leq y^+ \leq 5$. In the buffer layer the turbulence is progressively rising, $5 \leq y^+ \leq 30$, and the flow in the turbulent or log-law layer is turbulent, $y^+ \geq 30$.

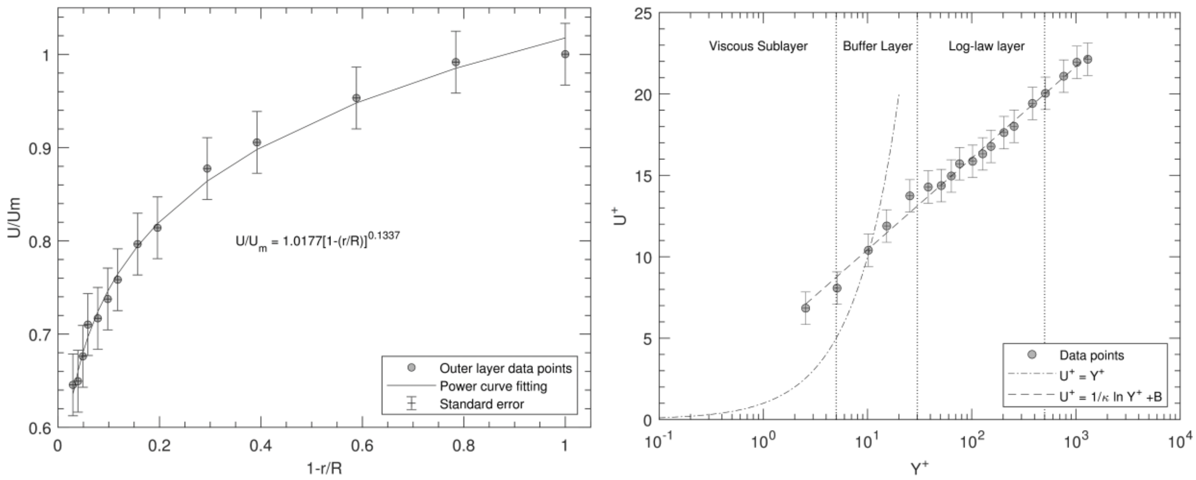

(a) Approximation of the normalised velocity fitted with the power-law curve.

(b) Dimensionless velocity profile showing the regions of the turbulent boundary layer.

Fig. 2: Experimental velocity profiles.

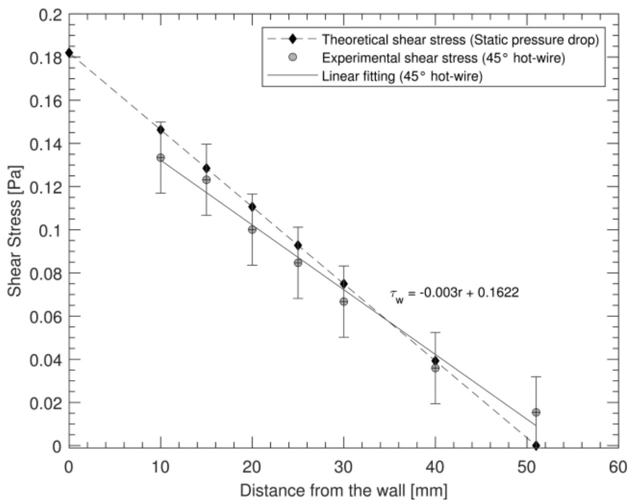

Fig. 3: Theoretical and experimental shear stress across the pipe.

3.1.2 Wall Shear Stress Analysis

Static pressure drop

The wall shear stress related to the pressure drop over a known length of the pipe was calculated by the pressure difference in mmH_2O. The value obtained from an analogue manometer is $2.7mmH_2O$ for a length of $3.81m$. Using equation (11), the wall shear stress measured by this method is found to be:

$$\tau_w = 0.182Pa$$

Mean Square Signal (45° Hot-wire)

The shear stress at the wall in this method was found by extrapolating the best fitted line of the experimental results. The linear best-fit equation, shown in Fig. 3, was used to find the value of the wall shear stress when $r = 0$.

Measurements of the RMS voltage have been taken at 10mm increments along the diameter of the pipe. The Reynolds shear stresses were obtained through equations (14) and (15) and the linear fit shear stress was computed by equation (16). Thus, the wall shear stress using the mean square signal of a hot-wire is estimated as:

$$\tau_w = 0.162Pa$$

Preston Tube

The wall shear stress was measured using a Preston tube, positioned so that its outer surface was tangential to the pipe wall, while facing upstream. An appropriate configuration of the analogue manometer enabled the dynamic pressure to be read. The pressure reading was $\delta P = 2.7mmH_2O$. Using equations (18) to (21), $X^* = 1.890$ and $Y^* = 1.927$ were obtained. Finally, equation (22) resulted in the following wall shear stress:

$$\tau_w = 0.188Pa$$

Clauser Plot

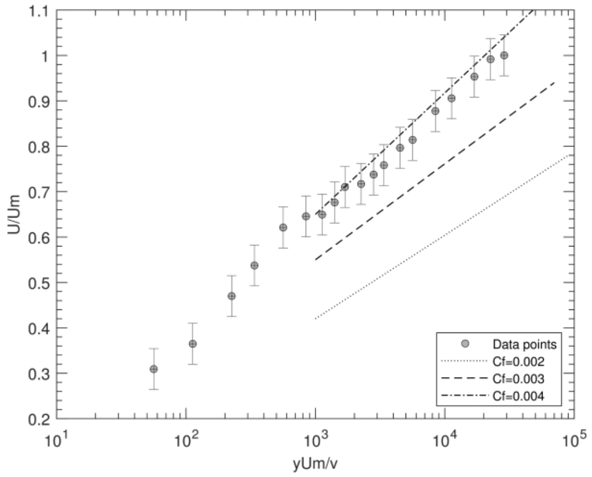

Fig. 4: Semi-logarithmic plot with different values of C_f from Sherman [44].

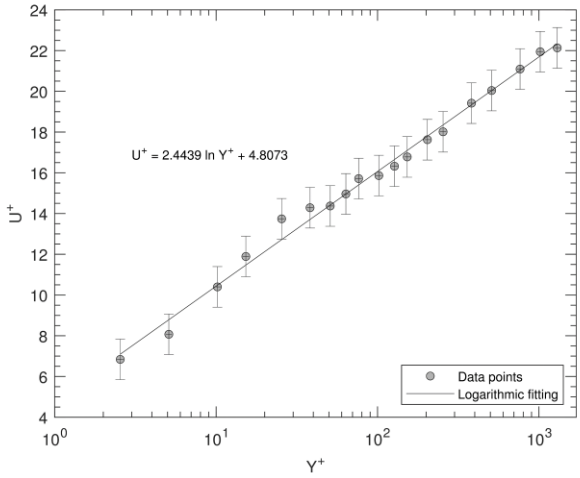

Fig. 5: Dimensionless velocity over dimensionless distance from the wall.

Fig. 4 represents the Clauser plot, illustrating that the line of best fit line is nearly aligned with the constant $C_f/2$ line at 0.002. Thus, the wall shear stress was calculated from equation (28), giving a wall shear stress value of:

$$\tau_w = 0.178Pa$$

Fig. 5 depicts the variation of the dimensionless velocity U^+ against the dimensionless distance Y^+, obtained from the data of the mean-square signal from a hot-wire. This graph is in agreement with the theory of the law of the wall or Clauser plot (Fig. 2b).

3.1.3 Error of Measurement

The margin of error in this work is reported to be within 2% in the hot-wire measurements of the mean velocity fluctuations using a CTA with linearizer [35]. The pressure error is the same order as the experimental uncertainty due to the difficult nature of turbulent flow over an orifice. The errors on hot-wire positioning and velocity measurements are $25\mu m$ and $0.25m/s$ respectively. Data points are accepted if they are between two to three times the reference profile of the error bars; if they are beyond this value, they are inconsistent. In this study, the data manages a close agreement with the reference solution, the mean pressure-gradient method, and all the experimental points obtained are consistent.

3.2 Computational Results

Analysis of different aspects of turbulence modelling, mesh independency and periodic boundary conditions helped to define the optimal parameters for a CFD simulation. The CFD simulation is validated against the data points obtained from the experiment using the mean square signal from a hot-wire method. One of the most important aspects to analyse is the sensitivity to the grid. The sensitivity test permits the CFD user to analyse the effects of fluid behaviour with the variation of a specific parameter in the simulation. A mesh independency study was carried out to examine the appropriate mesh to give an approximation of numerical error in the CFD simulation. In the present study, four significantly different grid resolutions were simulated and compared, producing remarkable data, shown in Table 3.

Table 3: Comparative table of mesh independency tests.

Turbulence model	k-ω SST			
Discretization Scheme	Second-order upwind			
Convergence Criteria	10^{-6}			
P-V Coupling Scheme	SIMPLE Scheme			
Boundary Conditions	- No-slip in the walls	- Periodic inlet/outlet		
Grid method	3D Multiblock - Hexahedral mesh			
Number of cells	3060 (coarse)	9520 (medium)	30240 (fine)	90045 (very fine)
Iterations to Converge	13589	4510	12914	26625
Maximum Wall Y+	0.053	0.028	0.028	0.025
CPU User time/Parallel*4	1463.88 s	764.764 s	4890.82s	55457.7 s
Wall clock	126.53 s	99.75 s	1016.62 s	13339.77 s
Mbytes used cells	3	9	29	77
Virtual Memory Usage	0.258 GB	0.279 GB	0.366 GB	0.414 GB

For the four different types of mesh simulated (Table 1), the medium mesh, 9520 cells, gave a good resolution that only differed 1% from the finest mesh and exhibited the same level of accuracy but with far lower computational times and memory usage. While it is generally assumed that significant improvements are always attained when refining the mesh [57], the results demonstrate that this is not always necessarily the case; with 9520 cells, the result is mesh independent. It is worth nothing that, despite the benefits of hexahedral cells, even this non-orthogonal cell can reduce the numerical stability of the solution and it can also produce a slower convergence [56].

A post-processing tool was used to generate the contour of velocity of the medium mesh with periodic boundary conditions and $\kappa - \omega - STT$ turbulence model. Measured at the outlet of the pipe, the contour shows that the lowest velocities can be found at the pipe wall while the highest velocities can be observed at the pipe centre and that the velocity progressively increases from $0 m/s$ for the former to $8.818 m/s$ for the latter, Table 4.

Table 4: Parameters for the simulation of the contour of velocity.

Parameter	**Value**	**Contour of velocity**
Pipe inner diameter	0.102 *m*	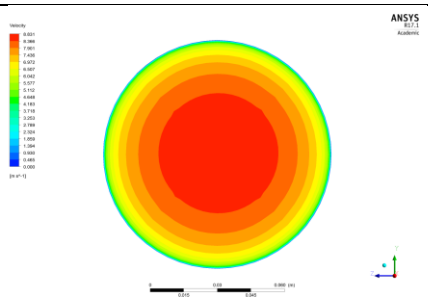
Length	0.004 *m*	
Reynolds number	57469	
Air density	1.19 kg/m^3	
Air viscosity	1.82×10^{-5} kg/ms	
Von-Karman constant	0.41 (±0.1)	
Mass flow rate	7.5×10^{-2} kg/s	
Velocity	7.5 *m/s*	
Nearest wall distance	3.43×10^{-5} m	

3.3 Experimental vs. Computational Results

3.3.1 Velocity profiles comparison

A comparison of the computational and experimental results for the velocity profiles across the pipe, presented on logarithmic axes in Fig. 6a for an easier assessment of the flow near the boundaries, indicates a satisfactory agreement between the two methodologies, with higher discrepancies appearing near the wall boundary. Moreover, a comparison of the dimensionless velocity profile across the pipe, shown in Fig. 6b, likewise denotes a good agreement between the experimental and computational results, albeit with some inconsistent values close to the wall due to the presence of the turbulence velocity.

3.3.2 Wall shear comparison

As with the velocity profile distribution, a comparison of the theoretical, experimental and computational results for the shear stress distribution across the pipe surface, as shown in Fig. 7, indicates a close agreement between the computational and experimental results. The CFD simulation produces almost identical results to the theoretical results close to the wall and near to the centreline, while small differences appear with the theoretical distribution in the region $1-\frac{r}{R} \in (0.61, 0.10)$; this region coincides with the region of the pipe where the velocity field deviates the most from the experimental results.

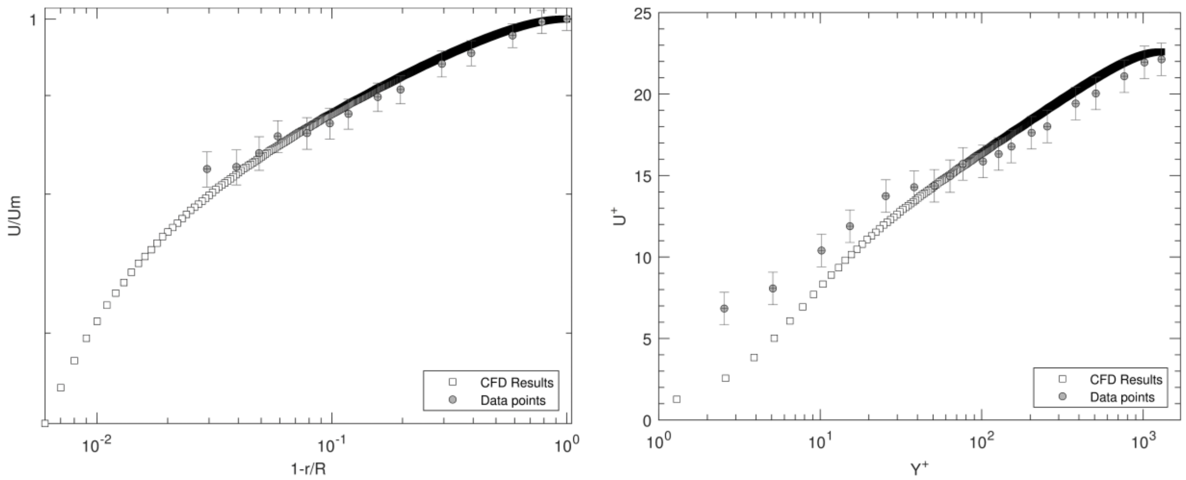

(a) Normalised velocity versus the dimensionless distance from the pipe wall on logarithmic axes.

(b) Dimensionless velocity U+ versus the dimensionless distance from the pipe wall Y+.

Fig. 6: Velocity profiles comparison between experimental and CFD results.

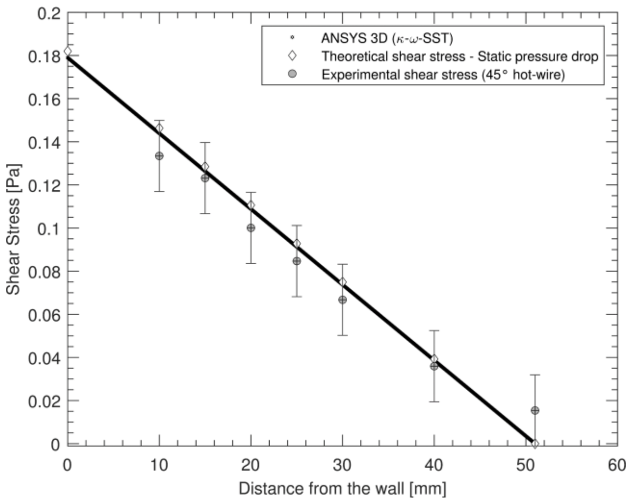

Fig. 7: Comparison of experimental, theoretical and CFD results of the shear stress distribution across the pipe.

3.4 Assessment of Errors

As the only direct method, the static pressure drop method is taken as a reference for assessing the validity of each method presented herein for the estimation of the wall shear stresses caused by fully developed turbulence flow. Table 4 displays a comparison between the experimental and computational results.

As illustrated, the CFD wall shear stress returns the closest agreement with the reference solution, with an error of approximately 1.6% compared to the experimental data. It is of interest to note that the CFD results are positioned exactly between the theoretical and experimental results of the mean square signal from a hot-wire method.

Table 5: Comparison of the experimental and computational methods for the calculation of wall shear stresses.

Method	**Wall shear stress [Pa]**	**Error**
Mean Pressure – Gradient method	0.182	Reference
3D CFD	0.179	+1.6%
The law of the wall	0.178	+2.2%
Preston tube	0.188	+3.3%
Mean square signal from a hot-wire	0.162	+10.4%

4 Conclusion

This paper has discussed the velocity profile and the mean shear stress in fully-developed turbulent pipe flow using air as working fluid and a Reynolds number of the order 50000. The flow has been considered as incompressible. Measurements have been conducted with four different methods and their results are in broad agreement. These results were compared with axisymmetric RANS simulation results obtained with a commercial CFD software package in which a combined $\kappa - \varepsilon$ / $\kappa - \omega - SST$ turbulence model was used. The model parameters and the initial and boundary conditions were given and the accuracy of the measurements were assessed by a comparison of the different approaches. This paper has demonstrated that, in all the experimental and computational methods tested here, the turbulent effects are well defined where there is interaction between the fluid and the wall. Importantly, it demonstrated that, while RANS is a slightly outdated approach that certainly does not capture all the flow physics of the laboratory measurements, for this particular case, with a high Reynolds number and utilising a standard computational turbulence model readily available with commercial packages, the numerical results produce a close agreement with the experiments. This demonstrates that, for certain cases, CFD simulations could be used as an alternative or complementary methodology to the experiments.

Acknowledgements The authors are grateful to Mr. Dennis Cooper and Dr Antonios Xenakis for their kind support and contributions.

References

1. Cengel, Y., Turner, R., Cimbala, J.: Fundamentals of Thermal-Fluid Sciences. McGraw Hill, New York (2008)
2. Perry, A.: Hot-wire anemometry. Oxford University Press, Oxford (1982)
3. Turns, S.: Thermal-Fluid Sciences. Cambridge University Press, Cambridge (2006)
4. Gad-el-Hak, M.: Advances in Fluid Mechanics Measurements. Springer-Verlag, Berlin (1989)
5. Head, M., Rechenberg, I.: The Preston tube as a means of measuring skin friction. Journal of Fluid Mechanics. 14, 1–17 (2006). https://doi.org/10.1017/S0022112062001020
6. Preston, J.: The determination of turbulent, skin friction by means of pitot tubes. Journal of the Royal Aeronautical Society. 58, 109–121 (1954)
7. Clauser, F.: The Turbulent Boundary Layer. Advances in Applied Mechanics. 4, 1–51 (1956). https://doi.org/10.2514/8.2938
8. Fernholz, H., Finley, P.: The Incompressible Zero-Pressure-Gradient Turbulent Boundary Layer: an Assessment of the Data. Progress in Aerospace Sciences. 32, 245–311 (1996). https://doi.org/10.1016/0376-0421(95)00007-0
9. Vardy, A., Brown, J.: Transient turbulent friction in smooth pipe flows. Journal of Sound and Vibration. 259, 1011–1036 (2003). https://doi.org/10.1006/jsvi.2002.5160

10. Reynolds, O.: An experimental investigation of the circumstances which determine whether the motion of water shall be direct or sinuous, and of the law of resistance in parallel channels. Philosophical Transactions of the Royal Society. 174, 935–982 (1883). https://doi.org/10.1098/rstl.1883.0029
11. Versteeg, H., Malalasekera, W.: An Introduction to Computational Fluid Dynamics. Pearson, London (1995)
12. Kapelson, A.: Computational of Mean Velocity Distribution in a Turbulent Flow. ARXIV Archive Website. https://arxiv.org/abs/physics/9904030 (1999). Accessed 12 November 2017
13. Launder, B., Spalding, D.: Mathematical models of turbulence. Academic Press, London (1972)
14. Menter, F.: Zonal Two Equation k-ω Turbulence Models for Aerodynamic Flows. 23rd Fluid Dynamics, Plasmadynamics, and Lasers Conference. 32, 1598–1605 (1993). https://doi.org/10.2514/6.1993-2906
15. Smagorinsky, J.: General Circulation Experiments with the Primitive Equations. Monthly Weather Review. 91, 99–164 (1963). https://doi.org/10.1175/1520-0493(1963)091<0099:GCEWTP>2.3.CO;2
16. Deardorff, J.: A numerical study of three-dimensional turbulent channel flow at large Reynolds numbers. Journal of Fluid Mechanics. 41, 453–480 (1970). https://doi.org/10.1017/S0022112070000691
17. Wahl, T.: Laboratory Calibration of the Mag-Tube Flow Meter. Water Resources Research Laboratory Report. PAP-904 (2003)
18. Boussinesq, M.: Calcul du pouvoir refroidissant des courants fluids. Journal de Math Pures et Appliques. 6, 285–332 (1905)
19. Russel, A.: The convection of heat from a body cooled by a stream of fluid. The London, Edinburgh, and Dublin Philosophical Magazine and Journal of Science. 20, 591–610 (1911). https://doi.org/10.1080/14786441008636941
20. King, L.: On the convection of heat from small cylinders in a stream of fluid: Determination of the convection constants of small platinum wires with applications to hot-wire anemometry. Proceedings of the Royal Society A: Mathematical, Physical and Engineering Sciences. 90, 373–432 (1914). https://doi.org/10.1098/rspa.1914.0089
21. Dryden, H., Kuethe, A.: The Measurement of Fluctuations of Air Speed by the Hot-Wire Anemometer. NASA Website. https://ntrs.nasa.gov/search.jsp?R=19930091390 (1929). Accessed 13 August 2018
22. Orszag, S., Patterson, G.: Numerical simulation of turbulence: Statistical Models and Turbulence. Springer-Verlag, Berlin (1972)
23. Craft, T.: Finite Difference Schemes. CFD Mechanical Aerospace and Civil Engineering Manchester Website. http://cfd.mace.manchester.ac.uk/twiki/pub/Main/TimCraftNotes_All_Access/cfd1-findiffs.pdf (2017). Accessed 16 July 2018
24. Pope, S.: Turbulent Flows. Cambridge University Press, Cambridge (2001)
25. Keshmiri, A., Cotton, M.A., Addad, Y., Laurence, D.: Turbulence Models and Large Eddy Simulations Applied to Ascending Mixed Convection Flows. Flow, Turbulence and Combustion. 89, 407–434 (2012). https://doi.org/10.1007/s10494-012-9401-4
26. Keshmiri, A.: Numerical sensitivity analysis of 3- and 2- dimensional rib-roughened channels. Heat and Mass Transfer. 48, 1257–1271 (2012). https://doi.org/10.1007/s00231-012-0968-z
27. Keshmiri, A., Cotton, M.A., Addad, Y., Rolfo, S., Billard, F.: RANS and LES investigations of vertical flows in the fuel passages of gas-cooled nuclear reactors. Proceedings of the 16th International Conference on Nuclear Engineering. 2, 297–306 (2008). https://doi.org/10.1115/ICONE16-48372
28. Keshmiri, A., Osman, K., Benhamadouche, S., Shokri, N.: Assessment of advanced RANS models against large eddy simulation and experimental data in the investigation of ribbed passages with passive heat transfer. Numerical Heat Transfer, Part B: Fundamentals. 69, 96–110 (2016). https://doi.org/10.1080/10407790.2015.1096641
29. Keshmiri, A., Uribe, J., Shokri, N.: Benchmarking of Three Different CFD Codes in Simulating Natural , Forced and Mixed Convection Flows. Numerical Heat Transfer, Part A: Applications. 67, 1324–1351 (2015). https://doi.org/10.1080/10407782.2014.965115
30. Keshmiri, A., Revell, A., Darabkhani, H.G.: Assessment of a common nonlinear eddy-viscosity turbulence model in capturing laminarization in mixed convection flows. Numerical Heat Transfer, Part A: Applications. 69, 146–165 (2016). https://doi.org/10.1080/10407782.2015.1069672
31. Hurst, D., Vassilicos, J.: Scaling and decay of fractal-generated turbulence. Physics of Fluids. 19, (2007). https://doi.org/10.1063/1.2676448
32. Chamorro, L., Porte-Agel, F.: A wind-tunnel investigation of wind-turbine wakes: Boundary-Layer turbulence effects. Boundary-Layer Meteorology. 132, 129–149 (2009). https://doi.org/10.1007/s10546-009-9380-8
33. Lomas, C.: Fundamentals of hot wire anemometry. Cambridge University Press, Cambridge (1986)
34. Bruun, H.H.: Hot-wire Anemometry: Principles and Signal Analysis. Oxford University Press, Oxford (1995)

35. Comte-Bellot, G.: Hot-Wire Anemometry. Annual Review of Fluid Mechanics. 8, 209–231 (1976). https://doi.org/10.1146/annurev.fl.08.010176.001233
36. Neu, M.: Hot-Wire and Hot-Film Anemometry. Virginia Tech Aerospace and Ocean Engineering Laboratory Website. http://www.dept.aoe.vt.edu/~simpson/aoe4154/hotwirelab.pdf (2011). Accessed 23 March 2021
37. Kudela, H.: Turbulent flow. Politechnika Warszawska Faculty of Mechanics and Energy Website. http://www.itcmp.pwr.wroc.pl/~znmp/dydaktyka/fundam_FM/Lecture_no3_Turbulent_flow_Modelling.pdf (2016). Accessed 13 August 2018
38. Harotinidis, J.H.: The measurement of wall shear stress. Advances in fluid Mechanics Measurements. 45, 229–261 (1989). https://doi.org/10.1007/978-3-642-83787-6_6
39. Tropea, C., Yarin, A., Foss, J.: Springer Handbook of Experimental Fluid Mechanics. Springer, Chicago (2007)
40. Kool, P.: Determination of the Reynolds-Stress Tensor with a Single Slanted Hot-wire in Periodically Unsteady Turbomachinery Flow. ASME International Gas Turbine Conference and Exhibit and Solar Energy Conference. (1979). https://doi.org/10.1115/79-GT-130
41. McDonough, J.: Introductory Lectures on Turbulence: Physics, Mathematics and Modeling. Mechanical Engineering Textbook Gallery Website. https://uknowledge.uky.edu/me_textbooks/2 (2007). Accessed 23 March 2021
42. Patel, V.: Calibration of the Preston tube and limitations on its use in pressure gradients. Journal of Fluid Mechanics. 23, 185–208 (1965)
43. Wei, T., Schmidt, R., McMurtry, P.: Comment on the Clauser chart method for determining the friction velocity. Experiments in Fluids. 38, 695–699 (2005). https://doi.org/10.1007/s00348-005-0934-3
44. Sherman, F.: Viscous Flow. McGraw-Hill, California (1900)
45. Salim, A., Salim, M.: Wall y+ Strategy for Dealing with Wall-bounded Turbulent Flows. Proceedings of the International MultiConference of Engineers and Computer Scientists. 2, 6 (2009)
46. Evola, G., Popov, V.: Computational analysis of wind driven natural ventilation in buildings. Energy and Buildings. 5, 491–501 (2006). https://doi.org/10.1016/j.enbuild.2005.08.008
47. Khier, W., Breuer, M., Durst, F.: Flow structure around trains under side wind conditions: A numerical study. Computers and Fluids. 29, 179–195 (2000). https://doi.org/10.1016/S0045-7930(99)00008-0
48. Kleinstreuer, C., Zhang, Z.: Laminar-to-turbulent fluid-particle flows in a human airway model. International Journal of Multiphase Flow. 2, 271–289 (2003). https://doi.org/10.1016/S0301-9322(02)00131-3
49. Umlauf, L., Burchard, H., Hunter, K.: Extending the k-w turbulence model towards oceanic applications. Ocean Modelling. 3, 195–218 (2003). https://doi.org/10.1016/S1463-5003(02)00039-2
50. Eggels, J., Unger, F., Weiss, M., Westerweel, J., Adrian, R., Friedrich, R., Nieuwstadt, F.: Fully developed turbulent pipe flow: A comparison between direct numerical simulation and experiment. Journal of Fluid Mechanics. 268, 175–209 (1994). https://doi.org/10.1017/S002211209400131X
51. Menter, F.: Two-Equations Eddy-Viscosity Turbulence Models for Engineering Applications. AIAA Journal. 32, 1598–1605 (1994). https://doi.org/10.2514/3.12149
52. ANSYS: 7.3.16 Periodic Boundary Conditions. ANSYS Website. www.afs.enea.it/project/neptunius/docs/fluent/html/ug/node252 (2009). Accessed 29 January 2018
53. Patankar, S.: Numerical Heat Transfer and Fluid Flow. Taylor & Francis, United States (1980)
54. Laurence, D.: Solving Linear Systems. MACE61040 Computational Fluid Dynamics, University of Manchester (2017)
55. Laufer, J.: The structure of turbulence in fully developed pipe flow. NASA Website. https://ntrs.nasa.gov/archive/nasa/casi.ntrs.nasa.gov/19930083975.pdf (1952). Accessed 13 August 2018
56. Craft, T.: Turbulence and Related Modelling. CFD Mechanical Aerospace and Civil Engineering Manchester Website. http://cfd.mace.manchester.ac.uk/twiki/pub/Main/TimCraftNotes_All_Access/ms4-turbflow.pdf (2010). Accessed 16 July 2018
57. Casey, M., Wintergerste, T.: European Research Community on Flow, Turbulence and Combustion] Special Interest Group on “Quality and Trust in Industrial CFD" Best Practice Guidelines. ERCOFTAC, London (2000)